Temperature-dependent resistivity of heavily doped silicon and germanium

Bo E. Sernelius
Department of Physics and Measurement Technology, Linköping University, S-581 83 Linköping, Sweden
(Received 21 September 1989)

We present a calculation of the temperature-dependent resistivity for heavily doped silicon and germanium. In addition to the contribution from impurity scattering, we include the contribution from electron-electron scattering, caused by the anisotropy of the conduction-band minima. The effects from this anisotropy on the impurity contribution are fully taken into account as well. We use the generalized Drude approach, which leads to results in closed form.

I. INTRODUCTION

A heavily doped semiconductor can for doping densities higher than n_c, the density of the metal-to-nonmetal transition, be viewed as an impure metal and behaves in many respects similar to an ordinary metal. However, the smallness of its Fermi energy E_F results in a much stronger response to external perturbations; since the Fermi energy decreases with decreasing doping density, this strong response is accentuated for densities near n_c. An applied magnetic field, e.g., might spin polarize all the carriers, while the strongest magnetic fields available in laboratories can flip the spins for a small fraction only of the electrons in an ordinary metal. This has dramatic effects on the magnetic susceptibility and the magnetoresistance of the doped semiconductors. For n-type doped silicon and germanium, the many-valley character of the conduction bands leads to a further reduction in the values of the Fermi energies. Near n_c the Fermi energies are much smaller than the Debye temperatures. This means that an interesting temperature dependence in, e.g., the transport properties can appear at low temperatures before phonon contributions set in. In the ordinary metals the phonon contributions dominate and mask the temperature dependence of other contributions.

In this work we are interested in the temperature dependence of the electrical resistivity. For both n-type silicon[1] and germanium,[2,3] close to n_c, the resistivity initially increases with temperature, has a maximum near T_F, the Fermi temperature, decreases, has a minimum, and increases again when the phonon contributions set in. For increasing donor density these structures gradually fade away and the resistivity increases monotonically with temperature. This behavior was initially considered anomalous and was together with a similar behavior of the Hall coefficient taken as strong support for the idea that the electrons were in an impurity band, situated below the conduction-band edge (for a review of these ideas see Ref. 4). Kurosawa *et al.*,[5] representing the competing idea that the electrons occupy the states in the host conduction band, proposed a phenomenological theory. They assumed that the resistivity was due to ionized impurity scattering and that the relaxation time $\tau(E)$ was a function of E/E_F, independent of both temperature and impurity concentration. By varying the functional form of $\tau(E)$ they could fit the temperature dependence of the resistivity for germanium quite well. Saso and Kasuya[6,7] managed to calculate the resistivity for germanium with the Boltzmann approach, taking the temperature-dependent screening into account. The anisotropy was partly included. They obtained qualitative agreement with experiments; also for the Hall coefficient. They extended the calculation to include nonlinear screening and effects from electron lifetime broadening and improved the agreement to semiquantitative.

In the present work we rely on the so-called generalized Drude approach[8] to obtain the temperature-dependent resistivity of heavily doped silicon and germanium. This approach has been found to work well for the contributions to the resistivity from phonon scattering,[9,10] impurity scattering,[11] and electron-hole scattering.[8] Here, the effects from the anisotropy on the impurity contribution are fully included. The anisotropy of the conduction-band valleys gives rise to extra scattering processes where two electrons from different valleys take part. This means an additional contribution to the resistivity. This contribution is included for the first time in the present calculation. Our approach has the advantages over the Boltzmann approach in that the electron-electron contribution can be obtained in the whole temperature range (not just in the quantum and classical limit[8,12]), and the results are obtained in closed form. The fact that electron-electron scattering can give contributions to the resistivity in anisotropic systems has been discussed before.[13–15] It has been considered in connection with semimetals,[16,17] and very crudely for many-valley semiconductors.[18]

In Sec. II we present the prescription for the generalized Drude approach and summarize the cases where its results have been compared to the results from more well-established approaches. Its success in reproducing results from other approaches is taken as an indirect proof of its validity. The derivation of the Drude expression for the dynamical conductivity and its high- and low-frequency expansions are presented in Sec. III. The high-frequency expression as obtained from the Kubo formalism is also given and $1/\tau(\omega)$ is identified. The numerical results are presented in Sec. IV. Section V, finally, contains a summary and conclusions.

II. THE GENERALIZED DRUDE APPROACH

The generalized Drude approach[8] (GDA) consists of three steps. In the first step the high-frequency limit of the dynamical conductivity is derived within the Kubo formalism and diagrammatic perturbation theory; in the second step, this result is compared to the high-frequency expansion of the generalized Drude expression for the dynamical conductivity and the relaxation time τ is hereby identified (the generalization of the Drude expression consists of allowing the relaxation time to be frequency dependent); in the third and last step the obtained expression for τ is assumed to be valid at zero frequency. This is a bold step, since τ was obtained from a high-frequency treatment.

The validity of the approach is not well established, since there is no strict, theoretical proof to back it up. However, there are indirect proofs or strong indications in favor of its validity.

In the case of impurity scattering[11,19,20] in a metallic system, GDA exactly reproduces the Ziman result[21] for the resistivity in impure metals. The elusive $(1-\cos\theta)$ factor, which is so difficult to reproduce[22] in a standard diagrammatic perturbation expansion based on the Kubo formalism, is here obtained automatically. Assuming that the obtained expression for τ is valid for all frequencies and not just for zero and high frequencies, the GDA exactly reproduces the result for the dynamical resistivity as obtained from the so-called energy-loss method.[23]

For acoustical-phonon scattering[24,25] in metals the GDA produces analytical results identical to those from Ziman's[26] solution to the Boltzmann equation.

Very recently GDA (Ref. 8) was used to calculate the resistivity from the electron-hole scattering in highly excited semiconductors. The results were compared to the numerical results from a Boltzmann approach.[12] Due to the very complicated situation, the Boltzmann approach could only be used in the quantum and classical limits. In those limits the GDA gave, as far as one could tell, identical numerical results. In the case of electron-hole scattering the GDA has the advantages over the Boltzmann approach in that it produces results in a closed form, and that the results are not limited to the classical and quantum limits.

However, one should mention that in all the cases discussed above only the lowest-order contribution to the high-frequency dynamical conductivity was included. The other approaches included only the lowest-order scattering events, as well. If the Born approximation is not good enough one should include higher-order contributions. Whether the GDA works also in that case has never been tested. We plan to investigate this in a future work. As mentioned in the Introduction the interesting structure in the temperature dependence of the resistivity increases in magnitude towards n_c. Unfortunately, the Born approximation works less well towards n_c, which means that we can only hope for qualitative agreement with experiments. We could improve the experimental agreement by using nonlinear screening along the lines of Ref. 7, but this will introduce uncertainties regarding the relative importance of impurity and electron-electron scattering. For the same reason we do not include phonon contributions. This means that our results for the resistivity will lack the upward curbing for higher temperatures. We should keep in mind that our results are the lowest-order contributions from impurity and electron-electron scattering.

III. DERIVATION OF THE DRUDE EXPRESSIONS AND APPLICATION OF THE GDA TO FIND THE STATIC RESISTIVITY

In this section we first derive the Drude expressions for the dynamical conductivity in heavily doped silicon and germanium and find its high-frequency expansions and zero-frequency limits. The high-frequency expansions are compared to the results from a derivation based on the Kubo formalism and diagrammatic perturbation theory, whereby the various relaxation times are identified. These are, following the prescription of the GDA, inserted into the zero-frequency limits of the conductivity. As a result we obtain the static conductivities and resistivities. Since the band structures of silicon and germanium are different we treat the semiconductors separately.

A. Silicon

The conduction band in silicon has band minima, valleys, in the six equivalent $\langle 100 \rangle$ directions inside the Brillouin zone (BZ). The valleys are anisotropic and the Fermi volumes are ellipsoids with their main axes pointing in the $\langle 100 \rangle$ directions. The energy dispersion around the bottom of the valleys are characterized by the longitudinal and transverse effective masses m_l and m_t, respectively; these have the values 0.9163 and 0.1905, respectively, and the background dielectric constant has the value 11.40. The anisotropy has the effect that at an applied electric field the carriers in each ellipsoid will, in general, have an average velocity not pointing in the direction of the field. However, due to the cubic symmetry, the total average velocity and current will point in the direction of the field and the magnitude will be independent of the direction. This means that we are free to choose the direction of the electric field at will. Let the field point in the (1,0,0) direction. This choice groups the carriers into two groups; group number 1, the carriers belonging to the two valleys in the $(\pm 1,0,0)$ directions, are characterized by the mass m_l; group number 2, the carriers belonging to the four valleys in the $(0,\pm 1,0)$ and $(0,0,\pm 1)$ directions are characterized by the mass m_t. Let the average velocities for the two groups be denoted by v_1 and v_2, respectively, and the corresponding relaxation times from impurity scattering by τ_1 and τ_2, respectively. The equations of motion for the two groups of carriers read

$$m_l v_1(-i\omega) = eE - \frac{m_l v_1}{\tau_1} - \eta \frac{2n}{3}(v_1 - v_2) \tag{3.1}$$

and

$$m_t v_2(-i\omega) = eE - \frac{m_t v_2}{\tau_2} - \eta \frac{n}{3}(v_2 - v_1) , \tag{3.2}$$

where n is the total carrier density, and η the coefficient of mutual friction. This coefficient is related to the relaxation time τ for scattering between the two groups of carriers. This relation is obtained from realizing that as the electric field and impurity scattering is turned off the relative velocity between the two groups of carriers decays with the decay constant $1/\tau$. For vanishing E, $1/\tau_1$, and $1/\tau_2$, Eqs. (3.1) and (3.2) reduce, after the inverse Fourier transform has been taken, into

$$\frac{dv_1}{dt}=-\eta\frac{2n}{3m_l}(v_1-v_2) \tag{3.3}$$

and

$$\frac{dv_2}{dt}=\eta\frac{n}{3m_t}(v_1-v_2)\ . \tag{3.4}$$

Subtracting the last of the two equations from the first leads to the following time dependence of the relative velocity:

$$(v_1-v_2)\propto\exp\left[-\eta n\frac{1}{3}\left[\frac{2}{m_l}+\frac{1}{m_t}\right]t\right]\ , \tag{3.5}$$

and τ can be identified as

$$\tau=\frac{1}{\eta n\frac{1}{3}\left[\frac{2}{m_l}+\frac{1}{m_t}\right]}\ . \tag{3.6}$$

Solving Eqs. (3.1) and (3.2), substituting η in favor of τ according to Eq. (3.6) and noting that the conductivity σ can be expressed as

$$\sigma=\frac{ne}{3E}(v_1+2v_2)\ , \tag{3.7}$$

we arrive at the following expression for the dynamical conductivity:

$$\sigma=\frac{\frac{ne^2}{\frac{1}{3}(2m_t+m_l)}\frac{1}{\tau}+\frac{ne^2}{3m_l}\left[\frac{1}{\tau_2}-i\omega\right]+\frac{2ne^2}{3m_t}\left[\frac{1}{\tau_1}-i\omega\right]}{\left[\frac{1}{\tau_1}-i\omega\right]\left[\frac{1}{\tau_2}-i\omega\right]+\frac{m_lm_t}{(2m_t+m_l)}\frac{1}{\tau}\left[\frac{2}{m_l}\left[\frac{1}{\tau_2}-i\omega\right]+\frac{1}{m_t}\left[\frac{1}{\tau_1}-i\omega\right]\right]}\ . \tag{3.8}$$

The high-frequency expansion of this expression is

$$\sigma\approx\frac{ne^2}{\omega^2}\left[\frac{1}{3m_l}\frac{1}{\tau_1}+\frac{2}{3m_t}\frac{1}{\tau_2}+\frac{2m_lm_t}{9}\frac{\left[\frac{1}{m_l}-\frac{1}{m_t}\right]^2}{\frac{1}{3}(2m_t+m_l)}\frac{1}{\tau}+i\omega\frac{1}{3}\left[\frac{2}{m_t}+\frac{1}{m_l}\right]\right],\quad \omega\to\infty\ , \tag{3.9}$$

and the zero-frequency result is found to be

$$\sigma(0)=ne^2\left[\frac{1}{3}\left[\frac{\tau_1}{m_l}+\frac{2\tau_2}{m_t}\right]-\frac{\frac{2}{9}\left[\frac{\tau_1}{m_l}-\frac{\tau_2}{m_t}\right]^2}{\frac{1}{3}\left[\frac{2\tau_1}{m_l}+\frac{\tau_2}{m_t}\right]+\tau\frac{1}{3}\left[\frac{2}{m_l}+\frac{1}{m_t}\right]}\right]\ . \tag{3.10}$$

We are further interested in two limits of Eq. (3.10), viz., the limit of vanishing *e-e* (electron-electron) scattering and that of infinite *e-e* scattering. These limits are

$$\sigma(0)=\frac{ne^2}{3}\left[\frac{\tau_1}{m_l}+\frac{2\tau_2}{m_t}\right],\quad \tau\to\infty \tag{3.11}$$

and

$$\sigma(0)=\frac{ne^2}{\frac{1}{3}\left[\frac{2m_t}{\tau_2}+\frac{m_l}{\tau_1}\right]},\quad \tau\to 0\ , \tag{3.12}$$

respectively. It is interesting to find that in the limit of extreme *e-e* scattering the conductivity depends only on the impurity scattering. The reason is that the *e-e* scattering determines the relative velocity between the two groups of carriers. In the extreme limit of strong *e-e* scattering both groups of carriers move with the same velocity and this velocity is determined by the impurity scattering. One should further notice that there is no resistivity at all in the absence of impurity scattering (since we have neglected the contribution from phonon scattering).

The high-frequency expansion of the Drude expression for the real part of the dynamical conductivity given in Eq. (3.9) consists of three terms, each containing one of the three different relaxation times; the first term is the impurity scattering contribution from the carriers of group 1; the second is the corresponding contribution from group 2; the last term comes from *e-e* scattering between the group 1 and group 2 carriers. The three different relaxation times are identified through a comparison with the corresponding results as obtained in Ref. 27. The first comparison [with Eq. (3.14) of Ref. 27] gives

$$\frac{ne^2}{\omega^2}\frac{1}{3m_l}\frac{1}{\tau_1} = \frac{e^4 n}{m_l^2 \kappa \omega^3 2\pi^2} \times \int d\mathbf{q}\cos^2(\mathbf{q},\hat{\xi})\mathrm{Im}\left[\frac{[2\alpha_1(\mathbf{q},\omega)-2\alpha_1(\mathbf{q},0)]}{\epsilon(\mathbf{q},\omega)\epsilon(\mathbf{q},0)}\right], \tag{3.13}$$

where $\hat{\xi}$, $\alpha_1(\mathbf{q},\omega)$, and $\epsilon(\mathbf{q},\omega)$ are the unit vector in the direction of the electric field, the polarizability from one of the two valleys belonging to group 1, and the total dielectric function, respectively. Please note that the polarizabilities in this work have κ, the background dielectric constant of the host in their denominators. Some further modifications made here are: The present expression is slightly less complicated from the fact that we here are dealing with a nonpolar semiconductor; we have further assumed random distribution of dopant ions, which means that the structure factor $S(q)$ in Ref. 27 is replaced by 1; since the polarizabilities are nonisotropic we have to keep the angular intergrations.

The total dielectric function is given by

$$\epsilon(\mathbf{q},\omega)=1+2\alpha_1(\mathbf{q},\omega)+2\alpha_2(\mathbf{q},\omega)+2\alpha_3(\mathbf{q},\omega)\ . \tag{3.14}$$

The polarizability from valley number i, $\alpha_i(\mathbf{q},\omega)$, can be expressed in terms of $\alpha_0(q,\omega)$, the corresponding polarizability in the case of isotropic band minima characterized by the density-of-states effective mass m_{de}. The relation is

$$\alpha_i(\mathbf{q},\omega)=\gamma^{-1/3}[1-(1-\gamma)\cos^2\vartheta_i] \times\alpha_0(q\gamma^{-1/6}[1-(1-\gamma)\cos^2\vartheta_i]^{1/2},\omega)\ , \tag{3.15}$$

where ϑ_i is the angle between $\mathbf{q}$ and the main axis of ellipsoid number i and $\gamma=m_t/m_l$. In the limit of zero frequency, Eq. (3.13) results in

$$\frac{1}{\tau_1(0)}=\frac{3e^2}{m_l\kappa\pi^2}\int d\mathbf{q}\cos^2(\mathbf{q},\hat{\xi})\frac{(d/d\omega)[\mathrm{Im}\alpha_1(\mathbf{q},\omega)]_{\omega=0}}{[1+2\alpha_1(\mathbf{q},0)+2\alpha_2(\mathbf{q},0)+2\alpha_3(\mathbf{q},0)]^2}\ , \tag{3.16}$$

where

$$\frac{d}{d\omega}[\mathrm{Im}\alpha_1(\mathbf{q},\omega)]_{\omega=0}=\frac{m_{de}^2e^2}{\kappa\hbar^3q^3\gamma^{-1/6}[1-(1-\gamma)\cos^2\vartheta_1]^{1/2}}\left\{1-\tanh\left[\frac{1}{2}\beta\left[\frac{\hbar^2q^2\gamma^{-1/3}[1-(1-\gamma)\cos^2\vartheta_1]}{8m_{de}}-\mu\right]\right]\right\}. \tag{3.17}$$

The parameter β is the usual temperature parameter $1/k_BT$, and μ is the chemical potential.

The relaxation time τ_2 is obtained in an analogous way with the result

$$\frac{1}{\tau_2(0)}=\frac{3e^2}{m_t\kappa\pi^2}\int d\mathbf{q}\cos^2(\mathbf{q},\hat{\xi})\frac{(d/d\omega)[\mathrm{Im}\alpha_2(\mathbf{q},\omega)]_{\omega=0}}{[1+2\alpha_1(\mathbf{q},0)+2\alpha_2(\mathbf{q},0)+2\alpha_3(\mathbf{q},0)]^2}\ , \tag{3.18}$$

where $\alpha_2(\mathbf{q},\omega)$ is the polarizability for one of the four valleys belonging to group number 2.

Finally, the relaxation time τ is obtained from the comparison of the third term in Eq. (3.9) with the zero-frequency limit of the first integral in Eq. (2.30) of Ref. 27. This gives

$$\frac{ne^2}{\omega^2}\frac{2m_lm_t}{9}\frac{\left[\frac{1}{m_l}-\frac{1}{m_t}\right]^2}{\frac{1}{3}(2m_t+m_l)}\frac{1}{\tau}=\frac{8e^2\hbar}{\omega^3}\left[\frac{1}{m_l}-\frac{1}{m_t}\right]^2\int_0^\infty\frac{d\omega_1}{2\pi}\frac{\hbar\beta\omega/2}{\sinh^2\hbar\beta\omega_1/2} \cdot\times\int\frac{d\mathbf{q}}{(2\pi)^3}q^2\cos^2(\mathbf{q},\hat{\xi})\frac{2\mathrm{Im}\alpha_1(\mathbf{q},\omega_1)\mathrm{Im}\alpha_2(\mathbf{q},\omega_1)}{|\epsilon(\mathbf{q},\omega_1)|^2}\ . \tag{3.19}$$

After rearrangement we obtain

$$\frac{1}{\tau}=\frac{36\hbar^2\beta}{n}\frac{1}{3}\left[\frac{2}{m_l}+\frac{1}{m_t}\right]\int_0^\infty\frac{d\omega_1}{2\pi}\frac{1}{\sinh^2\hbar\beta\omega_1/2}\int\frac{d\mathbf{q}}{(2\pi)^3}q^2\cos^2(\mathbf{q},\hat{\xi})\frac{\mathrm{Im}\alpha_1(\mathbf{q},\omega_1)\mathrm{Im}\alpha_2(\mathbf{q},\omega_1)}{|\epsilon(\mathbf{q},\omega_1)|^2}\ . \tag{3.20}$$

This completes the derivations of the relaxation times for silicon.

B. Germanium

The conduction band of germanium has anisotropic valleys in the X points, i.e., in the eight $\langle 111\rangle$ directions just at the BZ boundaries. This means that effectively four equivalent ellipsoidal Fermi volumes are filled with electrons in heavily doped germanium. The anisotropy is larger in germanium than in silicon and the ellipsoids are here cigar shaped, which means that *e-e* scattering is expected to be more important in germanium than in silicon. For Ge the effective masses m_l and m_t have the values 1.58 and 0.082, respectively, and κ the value 15.36.

Here we cannot, like we could for silicon, choose the direction of the field parallel to a symmetry axis for each ellipsoid. We choose the field to point in the (1,0,0) or $\hat{\mathbf{x}}$ direction, i.e., symmetrically with respect to all four ellipsoids. This has the effect that only one relaxation time appears from impurity scattering τ_{imp}, and one from *e-e* scattering τ. The average velocity is in each valley nonparallel to the average momentum. Hence, we have to keep the momenta in the equations of motion. The momentum and velocity of each ellipsoid will lie in the plane spanned by the main axis of the ellipsoid and the $\hat{\mathbf{x}}$ direction. Let p_1 and v_1 be the components of the momentum and velocity, respectively, in the $\hat{\mathbf{x}}$ direction, and p_2 and v_2 the modulus of the corresponding components in the $\hat{\mathbf{y}}$ and $\hat{\mathbf{z}}$ directions. The following relations between the v_i's and p_i's hold:

$$v_1=\frac{p_1}{3}\left[\frac{2}{m_t}+\frac{1}{m_l}\right]+\frac{2p_2}{3}\left[\frac{1}{m_l}-\frac{1}{m_t}\right], \tag{3.21}$$

$$v_2=\frac{p_1}{3}\left[\frac{1}{m_l}-\frac{1}{m_t}\right]+\frac{p_2}{3}\left[\frac{1}{m_t}+\frac{2}{m_l}\right]. \tag{3.22}$$

The equations of motion are identical for all valleys and are given by

$$p_1(-i\omega)=eE-\frac{p_1}{\tau_{\text{imp}}}, \tag{3.23}$$

$$p_2(-i\omega)=-\frac{p_1}{\tau_{\text{imp}}}-\eta n v_2 . \tag{3.24}$$

The first equation is the result in the $\hat{\mathbf{x}}$ direction and the second in the $\hat{\mathbf{y}}$ direction. The $\hat{\mathbf{z}}$ direction gives a redundant result.

For vanishing E and $1/\tau_{\text{imp}}$ Eqs. (3.22)–(3.24) give

$$\frac{dv_2}{dt}=-\eta n\frac{1}{3}\left[\frac{2}{m_l}+\frac{1}{m_t}\right]v_2 , \tag{3.25}$$

which leads to

$$v_2\propto\exp\left[-\eta n\frac{1}{3}\left[\frac{2}{m_l}+\frac{1}{m_t}\right]t\right] \tag{3.26}$$

and

$$\tau=\frac{1}{\eta n\frac{1}{3}\left[\frac{2}{m_l}+\frac{1}{m_t}\right]} . \tag{3.27}$$

Equations (3.22)–(3.24) and (3.27) give

$$p_1=\frac{eE}{1/\tau_{\text{imp}}-i\omega} , \tag{3.28}$$

$$p_2=-p_1\frac{\frac{1}{3}\left[\frac{1}{m_l}-\frac{1}{m_t}\right]}{\frac{1}{3}\left[\frac{2}{m_l}+\frac{1}{m_t}\right]}\frac{1/\tau}{1/\tau+1/\tau_{\text{imp}}-i\omega} , \tag{3.29}$$

and hence

$$\begin{aligned}\sigma&=\frac{nev_1}{E}\\&=ne^2\left[\frac{3}{(2m_t+m_l)}\frac{1}{1/\tau_{\text{imp}}-i\omega}\right.\\&\quad+\frac{2m_tm_l}{9}\frac{\left[\frac{1}{m_l}-\frac{1}{m_t}\right]^2}{\frac{1}{3}(2m_t+m_l)}\\&\quad\left.\times\frac{1}{1/\tau+1/\tau_{\text{imp}}-i\omega}\right] .\end{aligned} \tag{3.30}$$

The high-frequency expansion of this expression is

$$\sigma\approx\frac{ne^2}{\omega^2}\left[\frac{1}{3}\left[\frac{2}{m_t}+\frac{1}{m_l}\right]\frac{1}{\tau_{\text{imp}}}+\frac{2m_lm_t}{9}\frac{\left[\frac{1}{m_l}-\frac{1}{m_t}\right]^2}{\frac{1}{3}(2m_t+m_l)}\frac{1}{\tau}+i\omega\frac{1}{3}\left[\frac{2}{m_t}+\frac{1}{m_l}\right]\right], \quad \omega\to\infty , \tag{3.31}$$

and the zero-frequency result is found to be

$$\sigma(0)=ne^2\left[\frac{1}{\frac{1}{3}(2m_t+m_l)\frac{1}{\tau_{\text{imp}}}}+\frac{2m_lm_t}{9}\frac{\left[\frac{1}{m_l}-\frac{1}{m_t}\right]^2}{\frac{1}{3}(2m_t+m_l)}\frac{1}{\left[\frac{1}{\tau}+\frac{1}{\tau_{\text{imp}}}\right]}\right] . \tag{3.32}$$

The limit of vanishing *e-e* scattering is

$$\sigma(0)=ne^2\tau_{\text{imp}}\frac{1}{3}\left[\frac{2}{m_t}+\frac{1}{m_l}\right], \quad \tau\to\infty \tag{3.33}$$

and that of infinite *e-e* scattering

$$\sigma(0)=\frac{ne^2\tau_{\text{imp}}}{\frac{1}{3}(2m_t+m_l)}, \quad \tau\to 0 . \tag{3.34}$$

The high-frequency expansion of the Drude expression

for the real part of the dynamical conductivity given in Eq. (3.31) consists of two terms, each containing one of the two different relaxation times; the first term is the impurity scattering contribution; the second term comes from *e-e* scattering. The two different relaxation times are identified through a comparison with the corresponding results as obtained in Ref. 27. The first comparison [with Eq. (3.14) of Ref. 27] gives

$$\frac{ne^2}{\omega^2}\frac{1}{3}\left[\frac{2}{m_t}+\frac{1}{m_l}\right]\frac{1}{\tau_{\rm imp}}=\frac{2e^4n}{\kappa\omega^3\pi^2}\int\frac{d\mathbf{q}}{q^2}\left[q_x\frac{1}{3}\left[\frac{2}{m_t}+\frac{1}{m_l}\right]+(q_y+q_z)\frac{1}{3}\left[\frac{1}{m_l}-\frac{1}{m_t}\right]\right]^2 \times{\rm Im}\left[\frac{[\alpha_1(\mathbf{q},\omega)-\alpha_1(\mathbf{q},0)]}{\epsilon(\mathbf{q},\omega)\epsilon(\mathbf{q},0)}\right]. \tag{3.35}$$

Here and below we number the valleys with main axes in the (1,1,1), (1,−1,1), (1,1,−1), and (1,−1,−1) directions from 1 to 4 in the given order. The function $\alpha_i(\mathbf{q},\omega)$ is the polarizability from valley number i.

In the limit of zero frequency, Eq. (3.35) results in

$$\frac{1}{\tau_{\rm imp}(0)}=\frac{2e^2}{\kappa\pi^2\frac{1}{3}\left[\frac{2}{m_t}+\frac{1}{m_l}\right]}\int\frac{d\mathbf{q}}{q^2}\left[q_x\frac{1}{3}\left[\frac{2}{m_t}+\frac{1}{m_l}\right]+(q_y+q_z)\frac{1}{3}\left[\frac{1}{m_l}-\frac{1}{m_t}\right]\right]^2 \times\frac{(d/d\omega)[{\rm Im}\alpha_1(\mathbf{q},\omega)]_{\omega=0}}{[1+\alpha_1(\mathbf{q},0)+\alpha_2(\mathbf{q},0)+\alpha_3(\mathbf{q},0)+\alpha_4(\mathbf{q},0)]^2}. \tag{3.36}$$

Finally, the relaxation time τ is obtained from the comparison of the second term in Eq. (3.31) with the zero-frequency limit of the first integral in Eq. (2.30) of Ref. 27. This gives

$$\frac{ne^2}{\omega^2}\frac{2m_lm_t}{9}\frac{\left[\frac{1}{m_l}-\frac{1}{m_t}\right]^2}{\frac{1}{3}(2m_t+m_l)}\frac{1}{\tau}=\frac{16e^2\hbar}{9\omega^3}\left[\frac{1}{m_l}-\frac{1}{m_t}\right]^2 \times\int_0^\infty\frac{d\omega_1}{2\pi}\frac{\hbar\beta\omega/2}{\sinh^2\hbar\beta\omega_1/2} \times\int\frac{d\mathbf{q}}{(2\pi)^3} \times\frac{(q_y+q_z)^2{\rm Im}\alpha_1(\mathbf{q},\omega_1){\rm Im}\alpha_4(\mathbf{q},\omega_1)+2q_y^2{\rm Im}\alpha_1(\mathbf{q},\omega_1){\rm Im}\alpha_2(\mathbf{q},\omega_1)}{|\epsilon(\mathbf{q},\omega_1)|^2}. \tag{3.37}$$

Rearrangement gives

$$\frac{1}{\tau(0)}=\frac{4\hbar^2\beta}{n}\frac{1}{3}\left[\frac{2}{m_l}+\frac{1}{m_t}\right]^2\int_0^\infty\frac{d\omega_1}{2\pi}\frac{1}{\sinh^2\hbar\beta\omega_1/2} \times\int\frac{d\mathbf{q}}{(2\pi)^3}\frac{(q_y+q_z)^2{\rm Im}\alpha_1(\mathbf{q},\omega_1){\rm Im}\alpha_4(\mathbf{q},\omega_1)+2q_y^2{\rm Im}\alpha_1(\mathbf{q},\omega_1){\rm Im}\alpha_2(\mathbf{q},\omega_1)}{|\epsilon(\mathbf{q},\omega_1)|^2}. \tag{3.38}$$

This completes the derivations in this section.

IV. NUMERICAL RESULTS

In the previous section we derived all the necessary ingredients for the calculation of the temperature-dependent resistivity from impurity scattering and *e-e* scattering of heavily doped silicon and germanium. The polarizabilities entering the expressions are the retarded temperature-dependent RPA (random-phase-approximation) functions. Unfortunately, the real parts of these functions are not available in analytical form. However, the imaginary parts are.[28] In this work, the real parts have been obtained from the imaginary parts through the Kramers-Kronig dispersion relations. Since this is rather time consuming we have also calculated the results using the zero-temperature (analytical) versions of the real parts. This is to find out how far one can reach without invoking the full treatment.

In Fig. 1 we have collected the results from impurity scattering in Si at the donor density 4.0×10^{18} cm^{-3}. The relaxation times obtained from Eqs. (3.16) and (3.18) have been inserted into Eq. (3.11), and the resistivity is just the inverse of the conductivity. The full result (full effect from anisotropy and finite temperature) is presented as the solid curve. The long-dashed curve is the result when the zero-temperature screening is used. A comparison between the curves shows that the temperature-induced

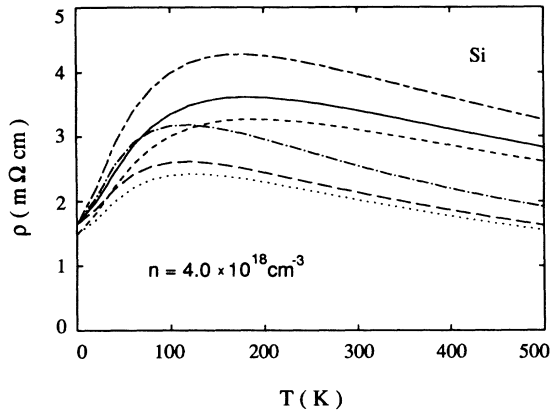

FIG. 1. The temperature-dependent resistivity from impurity scattering in silicon at a donor concentration of 4×10^{18} cm^{-3}. The solid and long-dashed curves are the results when the full anisotropy of the system has been taken into account exactly. For the solid curve the finite-temperature version of the real part of the dielectric function was used and for the long-dashed curve the zero-temperature version. The long-dashed-short-dashed and the dashed-dotted curves are the corresponding results for an isotropic approximation where the density-of-states effective mass was used to characterize the conduction-band dispersion. The short-dashed and dotted curves are the corresponding results when instead the optical effective mass was used.

reduction of the static screening (only static screening enters the impurity contribution) is important.

The other curves are for two common isotropic approximations. The long-dashed–short-dashed curve is

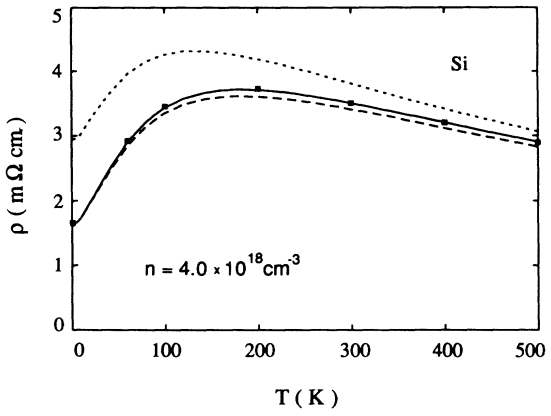

FIG. 2. The temperature-dependent resistivity in silicon at a donor concentration of 4×10^{18} cm^{-3}. The dashed curve is the same as the solid curve in Fig. 1, i.e., the contribution from impurity scattering when the effects from the anisotropy and the finite temperature are fully taken into account. The dotted curve is the result if maximum possible electron-electron scattering is present (see the text for details). The solid curve includes the actual electron-electron scattering contribution but the zero-temperature screening was used in this contribution. The solid squares are the results when the finite-temperature screening was used, and are hence the final results.

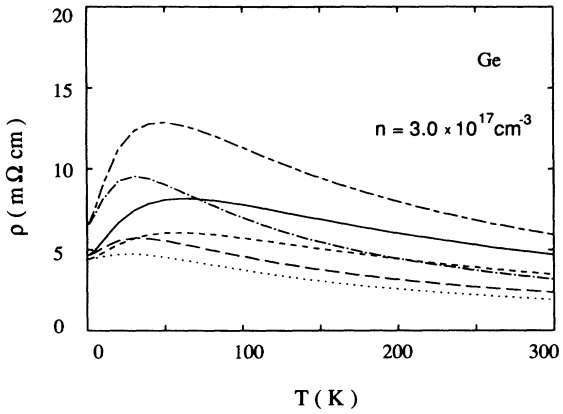

FIG. 3. The same as Fig. 1, but now for germanium at the donor concentration 3×10^{17} cm^{-3}.

the result from using the density-of-states effective-mass for the electrons and the long-dashed–dotted curve is the corresponding zero-temperature screening result. The short-dashed and dotted curve are the same, but are from using the optical effective mass. Krieger *et al.*[29,30] proposed that the big deviation between the experimental and theoretical magnitudes of the resistivity in many-valley semiconductors was due to very strong reduction in the screening due to the anisotropy. We can conclude from our results that this is not the correct explanation.

In Fig. 2 we have included the effects from *e-e* scattering. The dashed curve here denotes the full result from impurity scattering (solid curve of Fig. 1). Before the actual calculation of the *e-e* scattering effect it can be useful to see if the calculation is worth doing by studying the result from Eq. (3.12), which gives the maximum possible effect from *e-e* scattering. This result is shown as the dotted curve. The maximum effect is not negligible.

The full result is obtained from Eq. (3.10), where the

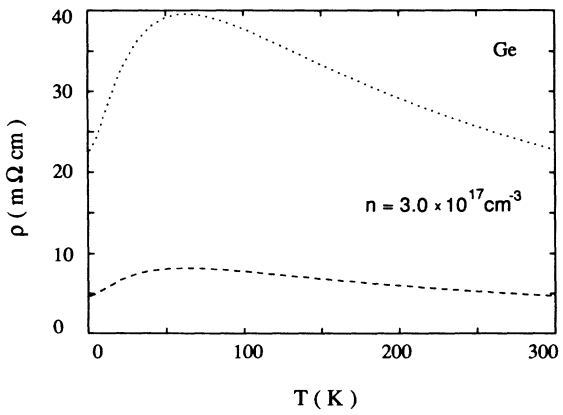

FIG. 4. The temperature-dependent resistivity in germanium at a donor concentration of 3×10^{17} cm^{-3}. The dashed curve is the same as the solid curve in Fig. 3, i.e., the contribution from impurity scattering when the effects from the anisotropy and the finite temperature are fully taken into account. The dotted curve is the result if maximum possible electron-electron scattering is present (see the text for details).

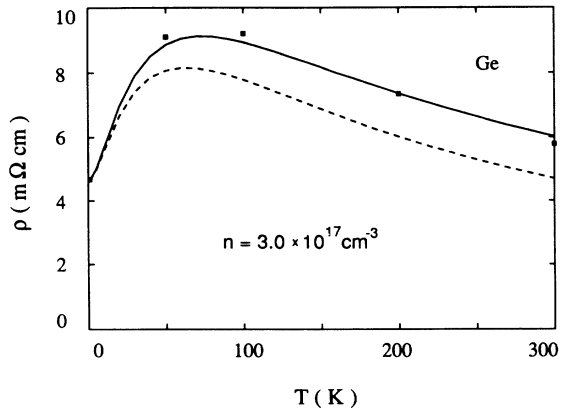

FIG. 5. The temperature-dependent resistivity in germanium at a donor concentration of 3×10^{17} cm^{-3}. The dashed curve is the same as in Fig. 4, i.e., the contribution from impurity scattering when the effects from the anisotropy and the finite temperature are fully taken into account. The solid curve includes the actual electron-electron scattering contribution, but the zero-temperature screening was used in this contribution. The solid squares are the results when the finite-temperature screening was used and are hence the final results.

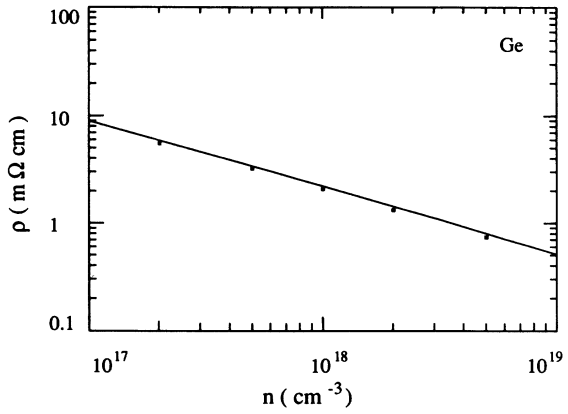

FIG. 6. Comparison between the results from the present GDA and the Boltzmann approach. The results are for the zero-temperature contribution to the static resistivity of heavily doped germanium as a function of donor density. The solid curve is the present result. The solid squares are the results from a numerical solution of the Boltzmann equation as obtained in Ref. 7.

additional relaxation time from *e-e* scattering is taken from Eq. (3.20). The result from the less-time-consuming version, using the zero-temperature screening, is given as the solid curve, and the full result from using the finite temperature screening as the solid squares. The temperature effects are much weaker in this case. The full result is slightly above the approximate one for low temperatures and slightly below for higher temperatures. The effects from *e-e* scattering are rather weak in silicon. Since the anisotropy is much stronger in germanium the effect should be stronger there.

In Fig. 3 we have collected the results from impurity scattering in germanium at the donor density 3.0×10^{17} cm^{-3}. The notation is the same as in Fig. 1. The results are from Eq. (3.33) with $\tau_{\rm imp}$ obtained from Eq. (3.36). Figure 4 demonstrates that *e-e* scattering might lead to a dramatic enhancement of the resistivity. The dotted curve is the result with maximum *e-e* scattering from Eq. (3.34), and the dashed curve is the result in absence of *e-e* scattering. The actual effect from *e-e* scattering is demonstrated in Fig. 5, where the notation is the same as in Fig. 2. The full result is from Eq. (3.32) with the relaxation time for *e-e* scattering taken from Eq. (3.38). As predicted, the effect is more important here than it was for silicon. The temperature effect on the screening is similar to in silicon.

Finally, we show in Fig. 6 a comparison between the results for the zero-temperature resistivity in germanium from this work (solid curve), and from a numerical solution to the Boltzmann equation as given in Fig. 1 of Ref. 7. The agreement is within five percent and this is probably the accuracy in the Boltzmann calculation. This comparison can be viewed as another test of the validity of the GDA. Unfortunately, only zero-temperature results from the "exact" solution to the Boltzmann equation were presented in Ref. 7. It would have been interesting to see how the methods compare for finite temperatures.

V. SUMMARY AND CONCLUSIONS

We have performed a calculation of the temperature-dependent resistivity for the many-valley semiconductors silicon and germanium. The calculation was performed with the generalized Drude approach. The effects from the anisotropy on the impurity contribution were fully taken into account. Included, as well, was the extra electron-electron scattering contribution induced by the anistropy. This contribution was found to be small for silicon, but important for germanium, where the anisotropy is bigger. The calculation was performed to the accuracy of the first Born approximation, which means that only qualitative agreement with experiments can be expected. We found the same temperature behavior as in experiments and in earlier calculations based on the Boltzmann approach; for densities near n_c, the resistivity increases with temperature, has a maximum for temperatures near the Fermi temperature, and then decreases again.

ACKNOWLEDGMENTS

Financial support from the Swedish Natural Science Research Council is gratefully acknowledged. We are further indebted to the National Supercomputer Center (NSC) at the University of Linköping for access to its Cray X-MP/48.

[1]C. Yamanouchi, K. Mizuguchi, and W. Sasaki, J. Phys. Soc. Jpn. **22**, 859 (1967).
[2]W. Sasaki, Suppl. Prog. Theor. Phys. **57**, 225 (1975).
[3]M. J. Katz, S. H. Koenig, and A. A. Lopez, Phys. Rev. Lett. **15**, 828 (1965).
[4]H. Fritzsche, in *The Metal Non-Metal Transition in Disordered Systems,* edited by L. R. Friedman and D. P. Tunstall (University of Edinburgh, SUSSP, Edinburgh, 1978).
[5]T. Kurosawa, M. Matsui, and W. Sasaki, J. Phys. Soc. Jpn. **42**, 1622 (1977).
[6]T. Saso and T. Kasuya, J. Phys. Soc. Jpn. **48**, 1566 (1980).
[7]T. Saso and T. Kasuya, J. Phys. Soc. Jpn. **49**, 578 (1980).
[8]Bo E. Sernelius, Phys. Rev. B (to be published).
[9]G. D. Mahan, *Many-Particle Physics* (Plenum, New York, 1981), Sects. 8.1A and 8.1G.
[10]G. D. Mahan, J. Phys. Chem. Solids **31**, 1477 (1970).
[11]Bo E. Sernelius and M. Morling, Thin Solid Films **177**, 69 (1989).
[12]M. Combescot and R. Combescot, Phys. Rev. B **35**, 7986 (1987).
[13]W. G. Baber, Proc. R. Soc. London, Ser. A **158**, 383 (1937).
[14]B. Jensen, Ann. Phys. **80**, 284 (1973).
[15]V. F. Gantmakher and I. B. Levinson, Zh. Eksp. Teor. Fiz. **74**, 268 (1978) [Sov. Phys.—JETP **47**(1), 137 (1978)].
[16]R. Hartman, Phys. Rev. **181**, 1070 (1969).
[17]C. A. Kukkonen and P. F. Maldague, Phys. Rev. Lett. **37**, 782 (1976).
[18]R. W. Keyes, J. Phys. Chem. Solids **6**, 1 (1958).
[19]Bo E. Sernelius, Phys. Rev. B **40**, 6218 (1989).
[20]Bo E. Sernelius and M. Morling, in *Shallow Impurities in Semiconductors,* edited by B. Monemar (IOP, Bristol, Philadelphia, 1989), p. 555.
[21]J. M. Ziman, *Principles of the Theory of Solids* (Cambridge University, New York, 1964), Chap. 7.
[22]G. D. Mahan, *Many-Particle Physics* (Plenum, New York, 1981), Sects. 7.1B and 7.1C.
[23]E. Gerlach, J. Phys. C **19**, 4585 (1986).
[24]G. D. Mahan, *Many-Particle Physics* (Plenum, New York, 1981), Sects. 8.1A and 8.1G.
[25]G. D. Mahan, J. Phys. Chem. Solids **31**, 1477 (1970).
[26]J. M. Ziman, *Electrons and Phonons* (Oxford University, New York, 1960).
[27]Bo E. Sernelius, Phys. Rev. B **36**, 1080 (1987).
[28]R. Sirko and D. L. Mills, Phys. Rev. B **18**, 4373 (1978).
[29]J. B. Krieger and T. Meeks, Phys. Rev. B **8**, 2780 (1973).
[30]J. B. Krieger, J. Gruenebaum, and T. Meeks, Phys. Rev. B **9**, 3627 (1974).